



CHORUS

This is the accepted manuscript made available via CHORUS. The article has been published as:

Testing the Jacob's ladder of density functionals for electronic structure and magnetism of rutile VO₂

Bing Xiao, Jianwei Sun, Adrienn Ruzsinszky, and John P. Perdew

Phys. Rev. B **90**, 085134 — Published 25 August 2014

DOI: [10.1103/PhysRevB.90.085134](https://doi.org/10.1103/PhysRevB.90.085134)

Testing the Jacob's Ladder of Density Functionals for Electronic Structure and Magnetism of Rutile VO₂

Bing Xiao, Jianwei Sun, Adrienn Ruzsinszky, and John.P. Perdew

Department of Physics, Temple University, Philadelphia, Pennsylvania, 19122, USA

Abstract

We employ semilocal density functionals (LSDA, PBE GGA, and meta-GGAs), LSDA+U, a nonlocal range-separated hybrid functional (HSE06), and the random phase approximation (RPA), to assess their performances for the ground-state magnetism and electronic structure of a strongly-correlated metal, rutile VO₂. Using recent quantum Monte Carlo results as the benchmark, all tested semilocal and hybrid functionals as well as RPA (with PBE inputs) predict the correct **magnetic ground states** for R-VO₂. The observed paramagnetism could arise from temperature-disordered local spin moments, or from the thermal destruction of these moments. All semilocal functionals also give the correct ground-state metallicity for R-VO₂. However, **in the ferromagnetic (FM) and anti-ferromagnetic (AFM) phases**, LSDA+U and HSE06 incorrectly predict R-VO₂ to be a Mott-Hubbard insulator. For the computed electronic structures of FM and AFM phases, we find that the TPSS and revTPSS meta-GGAs **give strong 2p-3d hybridizations, resulting in a depopulation** of the 2p bands of O atoms, **in comparison with** other tested meta-GGAs. The regTPSS, MGGA_MS0 and MGGA_MS2 meta-GGAs, which are free of the spurious order-of-limits problem of TPSS and revTPSS, give electronic states close to those of PBE GGA and LSDA. In comparison to experiment, semilocal functionals predict better equilibrium cell volumes for R-VO₂ in FM and AFM states than in the spin-unpolarized state. For meta-GGAs, a monotonic decrease of the exchange enhancement factor $F_x(s, \alpha)$ with α for small s , as in the MGGA_MS functionals, leads to large (probably too large) local magnetic moments in spin-polarized states.

PACS number(s): 71.15.Mb 71.27.+a 75.30.-m 75.47.Lx

I. INTRODUCTION

Vanadium dioxide (VO₂) exhibits an interesting temperature-induced first-order [1] phase transformation between two well-known polymorphs, namely monoclinic-VO₂ (M-VO₂) below 340K and rutile-type VO₂ (tetragonal crystal class) above 340K. The electronic structure changes significantly from M-VO₂ to R-VO₂. M-VO₂ is a non-magnetic insulator, and R-VO₂ is a paramagnetic metal [2]. The transition mechanisms from insulating M-VO₂ to metallic R-VO₂ are still under debate [2-14]. In some earlier works, using information obtained either from phonon dispersion or

electronic structure, the phase transition was found to be driven by the structural distortion or Peierls transition [2, 4-6]. This mechanism is supported by some experimental results [8, 9]. R-VO₂ is often considered to be a strongly-correlated transition metal oxide [3, 10-14]. Liebsch *et al.* [11] discussed the observed photoemission spectra of both R-VO₂ and M-VO₂, finding that the former VO₂ phase is a strongly correlated compound. Haverkort and coworkers [10] studied the changes of orbital occupation numbers due to the phase transition in VO₂ by measuring the V L_{2,3} XAS spectrum near the transition temperature. They found that the localization of 3d electrons is the prerequisite for occurrence of the Peierls distortions. Korotin *et al.* [3] calculated the electronic structures of both M-VO₂ and R-VO₂ using LSDA and LSDA+U methods. Their results strongly implied a Mott-Hubbard transition in this system. More recently, Eyert [4] applied the HSE06 functional to study the magnetism and electronic structures of VO₂ structures, finding that the HSE06 functional gave the better description for the ground state properties of VO₂ polymorphs, compared to semilocal functionals. However, Grau-Crespo *et al.* [12] revisited the magnetic structures and ground-state energies evaluated by the HSE06 functional. They concluded that HSE06 opens an insulating band gap for the metallic R-VO₂ phase, and that the obtained magnetic state is wrong for this structure. For example, the HSE06 functional significantly stabilizes the unobserved spin-polarized phases (ferromagnetic and anti-ferromagnetic states), and its results are even less realistic than the results computed by semilocal functionals tested previously. Gatti *et al.* [13] investigated the metal-insulator transition (MIT) in VO₂ system using the parameter-free GW method. Their calculations indicated that the inclusion of correlation effects is the key to correctly reproduce the MIT.

The conventional DFT methods are unable to describe the paramagnetic R-VO₂ phase, because local moments presumably exist and their directions are randomly distributed in real space. Those two features in a realistic paramagnetic (PM) phase are significantly different from the spin-compensated PM state. In the latter case, the local magnetic moment is exactly zero everywhere and its direction is undefined. The previous studies on M- and R-VO₂ systems are focused on the FM and AFM states [3, 4, 12]. The paramagnetic R-VO₂ is sometimes modeled as a spin-compensated PM state.

Interestingly, Zheng and Wagner [14] recently employed fixed-node diffusion quantum Monte Carlo (FN-DMC) simulations for both tetragonal and monoclinic VO₂ phases. They reported that FN-DMC predicts that the total energies of AFM and FM states are much lower than the spin-unpolarized reference for R-VO₂ in its ground state. Meanwhile, the energy difference between FM and AFM states in the same phase is in the range from 0 meV to 100 meV, depending on the computational parameters employed in the FN-DMC method such as nodal surface, cell size and time step. We may conclude that previous DFT calculations based on semilocal functionals (LSDA and PBE GGA) actually gave the qualitatively correct ground state and electronic structure for R-VO₂. On the other hand, the more elaborate

DFT+U and HSE06 functionals wrongly open an insulating gap in the partially-occupied 3d bands. In the picture suggested by the FN-DMC results, the local spin moments disorder at some temperature below 340K, and a Curie-Weiss law for the spin-susceptibility might be expected above the spin-disorder temperature. However, the magnetic susceptibility above 340 K has no observed dependence on temperature. The data do not allow us to apply the normal Curie-Weiss law to extract the transition temperature from the paramagnetic state to the possible ferromagnetic ordering somewhere below 340 K. Pouget and coworkers [15] also measured the magnetic susceptibilities of pure VO₂ and other samples doped with various amounts of Nb. For pure VO₂, their experimental magnetic susceptibility is the same as that of Ref. [1], and the Curie-Weiss law does not seem to apply to it.

The meta-GGA functionals and RPA are situated on the third and fifth rungs of Jacob’s ladder of density functional approximations, respectively [16-18]. Some meta-GGA functionals have been well-developed and tested for various properties of atoms, molecules and solids [17, 19-24]. The testing of non-empirically derived meta-GGA functionals for magnetic structures of solid is still very rare. In contrast, DFT+U and hybrid or fourth-rung functionals (PBE0 and HSE06) have already been applied to various strongly-correlated transition metal oxides [25, 26]. Due to its extremely high computational cost, the RPA has only been applied to realistic systems very recently [27-35]. VO₂ is considered as a model system for studying the phase transition involving electron-electron correlation. Therefore, we will apply several non-empirical meta-GGA functionals and RPA in this paper to calculate the magnetic and electronic structures of R-VO₂. We also compare our meta-GGA results with those of PBE and DFT+U. We find that the equilibrium cell volumes agree better with the observed cell volume for the paramagnetic metal when we assume ferromagnetic or anti-ferromagnetic phases than when we assume a spin-unpolarized phase. This result suggests either that there really are disordered local spin moments in R-VO₂, or that spin polarization is mimicking the energetic effect of strong correlation (as in DFT calculations for equilibrium Cr₂, or stretched H₂ [36]). Additionally, we find that the tested meta-GGA functionals of the Perdew family fall into two classes that perform differently for the magnetism of R-VO₂, i.e., the older TPSS and revTPSS functionals [20, 22], and the recently developed MGGA_MS family [37-40]. We have also analyzed the exchange enhancement factors of semilocal functionals, mostly meta-GGAs functionals, and have found that the magnetism of a solid is correlated with the behavior of the exchange enhancement factor $F_x(s, \alpha)$ of a meta-GGA for small s and large α . It is worth noting that the same range is also related to the description of van der Waals interaction between weakly-overlapped closed-shell systems [37-40]. Definitions of F_x , s , and α will be given in section IV.B. Results for monoclinic-VO₂ phase are not reported in this paper [41]. We could not test the exchange-correlation functionals of all five rungs on Jacob’s ladder for M-VO₂, because it has a bigger unit

cell than R-VO₂. We find that the HSE06 and RPA methods are too expensive for M-VO₂, and in practice the needed calculations are not doable with RPA using our current hardware.

II. COMPUTATIONAL DETAILS

The calculations were performed using the projector augmented wave (PAW) method in the Vienna *ab initio* simulation program (VASP) [42]. The PAW pseudopotentials employed in this work for V and O atoms were V_{3p3d4s} and O_{2s2p} within the frozen core approximation. The plane wave basis was expanded in the reciprocal space using a kinetic energy cutoff of 500 eV. The evaluations of ground-state energy and electron density were conducted in the first irreducible Brillouin zone using a 12×12×16 k-mesh of the Monkhorst-Pack type [43].

In this paper, we have considered the following meta-GGA-level exchange-correlation functionals: Tao-Perdew-Staroverov-Scuseria (TPSS) [20], revised TPSS (revTPSS) [22], regularized revTPSS (regTPSS) [44], meta-GGA made simple (MGGA_MS0 [37] and MGGA_MS2 [38, 39]). The first two meta-GGA functionals have been widely tested for various systems such as atoms, molecules and solids [17, 21]. The latter two functionals were devised recently in order to overcome some limitations of TPSS and revTPSS [39, 44]. Nevertheless, none of these non-empirically derived meta-GGA functionals has been tested for magnetic transition metal oxides. The calculations were also performed within the local spin density approximation (LSDA) using the Perdew-Zunger parametrization [45] and the generalized gradient approximation (GGA) of Perdew, Burke, and Ernzerhof (PBE) [46]. For the LSDA+U method [47], we have employed an implementation proposed by Dudarev [48] in the VASP code, and the effective $U_{eff} = 3.32$ eV ($U = 4.0$ eV and $J = 0.68$ eV) was used for 3d shells of the V atom [49]. Calculations using the range-separated hybrid functional HSE06 were also conducted for the different magnetic states of R-VO₂ [50-53]. Our calculation parameters were 400 eV for the kinetic energy cutoff and a 6×6×8 k mesh generated by the Γ -centered method, similar to those employed in Ref. [12]. The default range separation parameter ($\mu = 0.20 \text{ \AA}^{-1}$) for HSE06 in the VASP code was used in the current work [50-53].

For the RPA calculations, the total energy consists of two different terms, i.e., the correlation energy (E_c) and the Hartree-Fock energy (E_{HF}). In the current paper, R-VO₂ is considered as a metallic system when the inputs are obtained from PBE. For a metal, a special strategy must be employed to achieve numerical convergence [54, 55]. For example, the same k-mesh and kinetic energy cutoff must be used for calculating E_c and E_{HF} energies. Moreover, the $q \rightarrow 0$ part of the linear response function ($\chi_{G,G}(q,i\omega)$) was also omitted in evaluating the two energies. In our RPA calculations, the kinetic energy cutoff was set to 430 eV for FM and spin-compensated PM states, and to 480 eV for the AFM state, to reach convergence. The k-point mesh was similar to that employed for semi-local functionals. The convergence tests were

conducted for the calculated energy differences between magnetic and non-magnetic states of R-VO₂ by varying the kinetic energy cutoff and k grid. We found that a 6x8x8 k grid was sufficient to get the converged energy difference at a satisfactory numerical uncertainty ($\pm 10\text{meV}/\text{VO}_2$ (see Fig. SIII in Ref. [56]).

All DFT calculations were spin-polarized. For rutile-type VO₂, the calculations were carried out for three different magnetic configurations by assuming the local magnetic moments of V atoms in different magnitudes and directions, i.e., ferromagnetic (FM, with initial local magnetic moment set to $2\mu_B$), anti-ferromagnetic (AFM, with the same initial local moment as for FM) and spin-compensated paramagnetic (PM, with $0.1\mu_B$ as the initial local moment) states. Note that the spin-compensated PM state is different from a realistic PM phase. In the former case, the local moment is zero for each magnetic ion, because the majority and minority spin densities have the same magnitude at the same atomic site. The local moments carried by magnetic ions in the latter case are not only randomly distributed but also can vary strongly in magnitude. In Fig. 1, the crystal structure of rutile-VO₂ is illustrated for the FM and AFM states. Additionally, the experimental lattice constants of rutile-type VO₂ (R-VO₂) were used in our paper, i.e., $a=4.5546 \text{ \AA}$ and $c=2.8514 \text{ \AA}$ [2]. The internal geometric degrees of freedom of rutile-type VO₂ were optimized accordingly for each exchange-correlation functional **except RPA**. Using the current settings, the total energy was converged to 0.001 meV/atom and the mean Hellmann-Feynman force acting on the atoms was reduced to 0.01 eV/Å. **We also considered the effects of lattice constants on the computed energy differences by relaxing both lattice constants and atomic positions of R-VO₂ in FM, AFM and PM states. The PBE geometries were employed for all RPA calculations. Note that, unless stated otherwise, the results presented in this paper were calculated using experimental lattice constants with the optimized atomic positions.**

As can be seen from Fig. 2 (a), the local Cartesian coordinates of Vanadium atoms (V_I and V_{II}) in R-VO₂ are different from the global crystallographic Cartesian coordinates. In order to construct an interpretable angular-momentum-projected density of one-electron states, we have constructed the proper local 3d' (d'_{z^2} , $d'_{x^2-y^2}$, d'_{xy} , d'_{yz} and d'_{xz}) orbitals (in x-y-z coordinates) from the five 3d states (d_{z^2} , $d_{x^2-y^2}$, d_{xy} , d_{yz} and d_{xz}) of the global coordinates (X-Y-Z). Since the VO₆ octahedron in R-VO₂ has D_{4h} symmetry, the irreducible representations for the five 3d states under the local Cartesian coordinates are given by following relationship

$$\Gamma_5 = A_{1g}(d_{xy}) + B_{2g}(d_{yz}, d_{xz}) + B_{1g}(d_{xy}, d_{z^2}) + E_g(d_{xz}, d_{yz}, d_{x^2-y^2}) . \quad (1)$$

Here the irreducible representations A_{1g} , B_{2g} , B_{1g} and E_g denote the crystal field splitting of $3d^1$ with D_{4h} point group, as shown in Fig. 2(b). For each irreducible representation, a local d^1 state can be obtained from the linear combination of five normal d orbitals. The technical details are presented in the Ref. 56.

III. RESULTS

A. Stability of magnetism, and magnetic moments

Experimentally, the ground state of R-VO₂ above 340 K is a paramagnetic metal [1, 14, 15]. The electronic structure and magnetic state of quenched R-VO₂ below this temperature are unknown at the moment. Since DFT calculations are usually performed at 0 K, the direct comparison of the theoretical predictions with experiments is inappropriate. Fortunately FN-DMC results exist, and they imply that R-VO₂ is a magnetic metal in the ground state [14]. Therefore, we will use FN-DMC results as the benchmark in this work. Note that, from the FN-DMC results, the FM and AFM states have lower total energies than the PM state by approximately 300 meV/VO₂. One should be cautious about FN-DMC results, because the actual values are sensitive to the computational details [14]. Additionally, the exact energy difference between FM and AFM states is not available in the FN-DMC calculations.

The previous calculations based on either semilocal functionals (LSDA and GGA) or orbital-dependent DFT methods (HSE06) reproduce the correct ground-state magnetism of this phase using the experimental lattice constants [4, 12]. The obtained total energies of spin-polarized (FM and AFM) states are always lower than that of the spin-compensated PM state. For example, Williams *et al.* [57] have calculated the energy differences of R-VO₂ in magnetic states (AFM and FM) with respect to the non-spin polarized state. It was found that the energies of FM and AFM phases are lowered by 135 meV/VO₂ and 56 meV/VO₂ using the PBE GGA, compared to the non-spin-polarized phase. One should note that, in the works of Williams and coworkers [57], both the lattice constants and atomic positions were fixed to their experimental values. However, the atomic positions are allowed to relax in our calculations. HSE06 and DFT+U predict a much higher ground-state relative energy for PM R-VO₂ than PBE does [12].

We have applied the exchange-correlation functionals of all five rungs on Jacob's ladder (LSDA, LSDA+U, PBE, meta-GGAs, HSE06 and RPA) to calculate the energy differences between two magnetic states (FM and AFM) and the spin-compensated PM state. The results are given in Table I. Besides LSDA+U, other DFT methods predict the same ground magnetic phases as FN-DMC for R-VO₂, i.e., the FM and AFM states are always more stable than the spin-compensated PM state. Moreover, the FM state has a much lower energy than the AFM state. In the LSDA+U method, the AFM state is slightly more stable than the FM state by nearly 7 meV per VO₂ unit. The DFT+U method favors the strong localization of $3d$ electrons, and the electrons of R-VO₂ in the AFM state are more localized than in the FM state.

It is worth noting that the energy differences between magnetic and non-magnetic states given by LSDA+U and HSE06 are significantly more negative than those from semilocal functionals and RPA. Our HSE06 values are similar to those reported in Ref. 12. For RPA, the starting Kohn-Sham single-particle energies and orbitals were computed by PBE. The obtained energy difference by non-self-consistent RPA is close to PBE values in the FM state. Meanwhile, RPA stabilizes the AFM state more than PBE does. Nevertheless, non-self-consistent RPA with PBE inputs indeed shows that the ground state of R-VO₂ is a ferromagnetic metal. Among the five meta-GGA functionals, the FM and AFM states of R-VO₂ phase are strongly favored by MGGA_MS0 and MGGA_MS2, because the calculated energy differences between the two magnetic states and the PM state are significantly more negative than those from TPSS, revTPSS and regTPSS. TPSS and revTPSS give similar results for the calculated energy differences. The magnetization energies of regTPSS are slightly more negative than those of revTPSS and TPSS. Although LSDA also gives the lowest total energy for FM R-VO₂, the total energies of FM and AFM states calculated with LSDA are quite close to that of the spin-compensated non-magnetic state.

Using the fully relaxed **crystal structure**, we have recalculated the energy differences for R-VO₂ between magnetic phases (FM and AFM) and the PM state. The results are illustrated in Figs. 3 (a) and (b). We can see that the computed energy differences generally show a dependence on the geometry. Especially for LSDA+U and HSE06, the energy differences between magnetic states and the non-magnetic state are greatly reduced by using the optimized geometry. Additionally, LSDA+U now predicts lower energy for the FM state than for the AFM. It is also worth noting that LSDA now stabilizes the spin-compensated PM state over the AFM state (see the computed values given in Table SI in Ref. 56), i.e., the total energy of the AFM state is slightly higher than that of the PM state by 0.08 meV per VO₂. Meanwhile, the total energy of the FM state is almost identical to that of the non-magnetic phase in LSDA. Moreover, the relative stability of the PM state is comparable to that of the AFM state for most semilocal functionals. Using the optimized geometries, RPA values are now less negative than those obtained from experimental crystal structures. In summary, in the fully relaxed case, all tested density functional methods give the correct **magnetic ground states** for R-VO₂ in agreement with the FN-DMC simulation for the ground state.

In Fig. 4, the calculated total magnetic moments of V atoms are given according to their Wyckoff positions. For R-VO₂, the covalent state of V is +4, implying a $3d^1$ configuration. Therefore, the nominal magnetic moment of V is $1 \mu_B$. Our calculations for the FM state of R-VO₂ are roughly in agreement with this conjecture for all tested density functionals. One should note that the obtained magnetic moments of V atoms by MGGA_MS0, MGGA_MS2, LSDA+U and HSE06 for R-VO₂ in the FM state are larger than $1 \mu_B$. Note that the exact local magnetic moment of the V atom in R-VO₂ is currently unknown both theoretically and experimentally. Our best (but questionable) standard is

provided by revTPSS: 1.0-1.1 μ_B in the FM state, and 0.4 μ_B in the AFM state. We choose revTPSS as our standard because Sun *et al.* [58] have tested TPSS and revTPSS for the magnetic moments of Fe and Ni in ferromagnetic states, obtaining results in good agreement with experiment. In Ref. 14, it is also suggested that the local magnetic moment of R-VO₂ in the FM state is nearly 1.1 μ_B by the FN-DMC method. Taking the revTPSS magnetic moment as a standard, LSDA and TPSS slightly underestimate the local moments in the FM state, while the MGGA_MS variants, LSDA+U, and HSE06 all overestimate them. We find that RPA gives exactly 1 μ_B in the ferromagnetic state. In the FM state, the RPA local moment for the V atom was obtained by minimizing the total cell energy with respect to magnetic moment, based on constrained PBE inputs (orbitals and local magnetic moments) (see Fig. SII in Ref. 56).

For the AFM state, the semilocal functionals, LSDA, PBE, TPSS, revTPSS and regTPSS predict much smaller magnetic moments for V atoms than the MGGA_MS variants do. The values from the former exchange-correlation functionals are only 30%~50% of those of the other functionals (LSDA+U, MGGA_MS0, MGGA_MS2 and HSE06). A small local magnetic moment in the AFM state implies that the spin-up and spin-down components nearly compensate one another, resulting in an electron distribution similar to that of the spin-compensated PM state. The local moments obtained by LSDA+U, MGGA_MS2 and HSE06 are close to the nominal value of 1 μ_B for the free V⁴⁺ cation. Again taking revTPSS as our standard, it appears that the MGGA_MS variants and the more elaborate functionals overestimate the local magnetic moment in the AFM as in the FM state. But a more reliable standard is needed.

B. Electronic structures

The weighted band dispersions of ferromagnetic R-VO₂ in the up-spin direction are shown in Fig. 5 for the PBE, TPSS, MGGA_MS2 and HSE06. In Ref. 56, we also display the results computed by other DFT methods such as LSDA, LSDA+U, revTPSS and regTPSS in Figs. SV-SVIII. The results for the spin-down electrons are quite similar to those of the up-spin channel except that the band energies are shifted due to the exchange splitting. The unit cell of R-VO₂ has two VO₂ structural units, implying that the total number of bands in each spin channel is doubled, compared to one VO₂ formula unit. In our plots, the four lowest lying bands (below -15 eV) mainly consist of 2s orbitals of O atoms. The 2s bands are less dispersive and their band energies are also far below the Fermi level. Therefore, the overlap of 2s orbitals between atoms are expected to be negligible. From Fig. 6, we find that meta-GGAs predict more negative energy for 2s bands than LSDA, LSDA+U and PBE. Among meta-GGAs, MGGA_MS0 and MGGA_MS2 give less negative band energy than TPSS, revTPSS and regTPSS for 2s orbitals. Meanwhile, MGGA_MS variants also predict narrower band widths for 2s orbitals than other functionals. The main reason why meta-GGAs tend to lower the 2s band energy can be explained using their exchange enhancement factors in the limit of small s when α is zero. Unlike LSDA

and PBE, the meta-GGAs tested in this paper use α to distinguish the single-orbital region ($\alpha=0$) from the uniform electron gas ($\alpha=1$) having the same s [16, 20, 22, 39]. In the single-orbital region, we have $\alpha=0$ and small s . The exchange gradient enhancement factor in a meta-GGA is always larger than those of LDA and PBE in such cases. Therefore, meta-GGAs lower the energy of the $2s$ orbital below that of the latter functionals.

The valence bands of R-VO₂ are dominated by $2p$ orbitals of O atoms. In our simulated crystal structure, each spin direction has 12 electronic bands. Except for RPA, the average eigenenergy and band position of the $2p$ bands are calculated for each functional at the Γ point in the first Brillouin zone, and the results are listed in Table SIII [56]. The computed band positions indicate that the TPSS value is too high and revTPSS is too low. The remaining functionals give similar values for this quantity.

It can be clearly seen from Fig. 5 that the conduction bands of R-VO₂ are mainly attributed to $3d$ states of V atoms. Without considering the tetragonal distortion of VO₆ octahedra (O_h point group), the lower part of the d bands is made of six T_{2g} type orbitals (d'_{xy} , d'_{yz} and d'_{xz}). Otherwise, the upper d bands consist of four other E_g type orbitals (d'_{z^2} and $d'_{x^2-y^2}$). The band gap of E_g-T_{2g} splitting due to O_h (or D_{4h}) crystal field for $3d$ states in R-VO₂ was described in some previous works [2-4, 6]. In our calculations, part of the T_{2g} band is always overlapped with the E_g bands. Therefore, no obvious crystal-field-created band gap can be observed between the E_g and T_{2g} bands. The mixture of $3d$ bands with $2p$ states determines the strength of V-O covalent bonds in the structure. For TPSS and revTPSS, the $2p$ - $3d$ hybridizations are significantly stronger than for other tested functionals, which is clearly illustrated in the calculated $3d$ weighted band dispersions in Fig. 5 and also in the electron populations given in Fig. SIX in Ref. 56. For example, all $2p$ bands predicted by revTPSS and TPSS exhibit a strong $3d$ character. Meanwhile, the $3d$ bands are populated with more electrons than those of other semilocal and nonlocal functionals. **We should note that there is no decisive experimental result available at the moment for the electronic structure of R-VO₂. Therefore, strong $2p$ - $3d$ hybridization in TPSS or revTPSS calculation cannot be totally ruled out.**

In the case of PBE+U and HSE06, the band gap is opened between occupied and unoccupied $3d$ states. As a result, in LSDA+U and HSE06 calculations, R-VO₂ is a Mott insulator in the FM and AFM states (see Figs. SV-SVIII in Ref. 56).

In R-VO₂, the actual point group of a VO₆ octahedron is D_{4h}, resulting in the splitting of T_{2g} and E_g states further according to Eq. 1. Specifically, the correct ordering of five $3d'$ states in FM R-VO₂ is given in Fig. 2 (b) as E_g (d'_{xz} , d'_{yz}) < B_{1g} (d'_{xy}) < A_{1g} (d'_{z^2}) < B_{2g} ($d'_{x^2-y^2}$). From Eqs. (S7) and (S8) in Ref. 56, in the local coordinates, d'_{z^2} and

$d_{x^2-y^2}$ only show T_{2g} ($B_{1g} + E_g$) symmetry in an undistorted VO_6 octahedron. Meanwhile, the linear combinations of d_{xy} , d_{yz} and d_{xz} can have both T_{2g} ($B_{1g} + E_g$) and E_g ($A_{1g} + B_{2g}$) characters. The angular momentum projected local densities of states of FM R- VO_2 are shown in Fig. 7 for the tested semilocal and nonlocal functionals. The Kohn-Sham single-particle energies of five $3d$ states (d_{xy} , d_{yz} , d_{xz} , d_{z^2} and $d_{x^2-y^2}$) and their relative positions in Fig. 7 are generally in agreement with the ordering of local $3d$ states constructed from Eqs. (S7) and (S8) using group theory. Our current results also agree with Ref. 54. Finally, it is worth noting that, in the [001] direction, the sublattice of V atoms can form d-d σ -bonds through the overlapping of d'_{xy} (B_{1g}) orbitals between the nearest unit cells, and this has been considered as one possible driving force for tetragonal VO_2 transforming into the monoclinic phase at low temperature (below 340 K) [1, 2].

The computed electronic densities of states by different DFT methods for the FM state are shown in Fig. 7, and for the AFM and spin-compensated PM phases in Fig. SVII [56]. The electronic structures of AFM and PM states resemble those of the FM phase. The discussions are omitted here for brevity.

IV. DISCUSSION

A. Error cancellation of semilocal functionals in a strongly-correlated system; unit cell volume

The likeliest interpretation of our results, in light of previous works [1, 14, 15], is that the observed paramagnetism of R- VO_2 arises from temperature-disordered local moments. However, an alternative interpretation is that R- VO_2 is a spin-compensated but strongly-correlated paramagnetic metal, in which the magnetic states found in DFT simply mimic the energetic effects of strong correlation [36].

Sometimes standard density functionals can imitate strong correlation by developing a spin polarization [32]: The extra exchange then keeps the electrons apart in the same way that strong correlation does. The classic example is the stretched H_2 molecule. LSDA and GGA descriptions wrongly localize the spin-up electron on one site and the spin-down on the other, but this leads to a nearly correct energy. Using the correct spin-unpolarized singlet density of stretched H_2 (spin-compensated PM state in our case) leads to an energy that is much too high. As a consequence, it is expected that the ground-state energy and equilibrium cell volume of R- VO_2 computed in an energy-minimized magnetic phase should be more accurate than those computed in the spin-compensated PM state. In Fig. 8, we show the calculated percent errors of different DFT methods for the equilibrium cell volume. It is generally true that the AFM and FM calculations predict better lattice geometry than that of the spin-compensated PM case except for LSDA and

RPA. One special case is the PBE functional for which the cell volume obtained for the AFM state is almost the same as for the spin-compensated PM state, and both values are in good agreement with the experimental value. Otherwise, the optimized cell volumes of R-VO₂ by TPSS, revTPSS and regTPSS in the AFM state are identical to the corresponding values in the PM state. Since the local magnetic moments given by LSDA, PBE, TPSS, revTPSS and regTPSS are significantly smaller than those of other tested DFT methods (LSDA+U, HSE06 and two MGGA_MS variants), the ground-state electron density distribution of the AFM state predicted by them is close to that of a spin-compensated PM solution. Therefore, for LSDA, PBE, TPSS, revTPSS and regTPSS, the ground-state energy and equilibrium cell volume in AFM state do not differ too much from those of the spin-compensated PM state. For LSDA, the predicted local spin magnetic moments are too small for both FM and AFM phases, indicating that the spin-compensated PM state is more favored by this functional than by other semilocal functionals. As a result, the obtained percent errors for cell volume in three different magnetic states are similar to each other.

The RPA optimized cell volume can be obtained by minimizing the total RPA energy as a function of PBE cell volume through fitting of the equation of state (EOS), **fixing the c/a ratio to the experimental value and the internal degrees of freedom to PBE results**. We find that this geometry optimization procedure gives a very poor equilibrium cell volume for all three R-VO₂ magnetic states. In contrast to the tested semilocal functionals, LSDA+U and HSE06, accurate cell volumes are not found from a spin-polarized state for RPA. One possible explanation is that the current RPA is not implemented self-consistently.

Previous studies [31-35] showed that RPA energy differences can **be sensitive to the DFT inputs**. Our RPA results are based on PBE orbitals and orbital energies. It would be interesting to employ instead selfconsistent **RPA orbitals or inputs from other semilocal (meta-GGAs) and non-local (HSE family or PBE0) exchange-correlation functionals in the future**. The large difference between spin-up and -down channels in the exchange potential can be significantly reduced by adding the correlation potential in the selfconsistent RPA+EXX method [60, 61]. However, selfconsistent RPA is not available yet in VASP.

B. Analysis of the effects of the exchange enhancement factor

Although different semilocal functionals may have different correlation parts, it is often possible to correlate their differences in performance to differences in their plottable exchange enhancement factors $F_x(s, \alpha)$.

In a meta-GGA, the total exchange energy of a spin-unpolarized density is computed as

$$E_x[n] = \int n \mathcal{E}_x^{unif}(n) F_x(s, \alpha) d^3r, \quad (2)$$

where n is the total electron density ($n_\uparrow = n_\downarrow = n/2$) and $\epsilon_x^{unif}(n)$ is the exchange energy per particle of uniform electron gas. The exchange energy $E_x[n_\uparrow, n_\downarrow]$ of a spin-polarized density follows from Eq. (2) via a spin-scaling relation [46]. The exchange enhancement factor over LDA, a function of both s and α , is given by $F_x(s, \alpha)$ [20, 22, 37-39]. The two ingredients (s and α) in $F_x(s, \alpha)$ are defined as:

$$s = \frac{|\nabla n|}{2(3\pi^2)n^{4/3}}, \quad (3)$$

$$\alpha = \frac{\tau - \tau_W}{\tau_{unif}}. \quad (4)$$

In Eq. 4, the orbital kinetic energy density $\tau = \sum_\sigma \tau_\sigma$ with $\tau_\sigma = \frac{1}{2} \sum_i |\nabla \phi_{i\sigma}|^2$; $\tau_W = |\nabla n|^2 / 8n$ is the von Weizsäcker kinetic energy density, which is exact for one- and two-electron densities; $\tau_{unif} = \frac{3}{10} (3\pi^2)^{2/3} n^{5/3}$ represents the kinetic energy density of the uniform electron gas. s is the dimensionless or reduced density gradient, present even in GGAs, while α is the dimensionless deviation from a single orbital shape, present only in meta-GGAs.

First, we note that the TPSS and revTPSS meta-GGA's, unlike the other semilocal functionals considered here, display an unphysical order-of-limits error in which the value of $F_x(s=0, \alpha=0)$ depends on which ingredient is taken first to zero. We have already seen in section III.B that TPSS and revTPSS predict **strong hybridization** of O $2p$ with V $3d$ orbitals, in comparison with the band structures of the other semilocal functionals. One might attribute this excess hybridization to the order-of-limits error in TPSS and revTPSS [44], although we have no physical explanation for this.

We plot the enhancement factors of LDA, PBE, and several meta-GGAs as functions of α in Fig. 9. In meta-GGAs, α is used to distinguish different orbital regions and chemical bonds [39]. For the PBE GGA, the gradient enhancement factor does not depend on α ; its value is explicitly determined by the reduced density gradient (s) only. Therefore, it is represented by a horizontal line for each s in plots of $F_x(s, \alpha)$ versus α . Moreover, the LDA enhancement factor $F_x = 1$ is independent of both s and α , implying that it is represented by a horizontal line with a value of unity. In Table. SV, the exchange enhancement factors of five meta-GGAs in different limits are summarized [56].

In Fig. 4, we found that MGGA_MS0 and MGGA_MS2 predict much larger local magnetic spin moments than the other semilocal functionals do (and too large in comparison with our uncertain standard, revTPSS). Fig. 9 shows that MGGA_Ms0 and MGGA_MS2 are also distinguished by a monotonic decrease in $F_x(s, \alpha)$ with α at small s . Our results suggest that the limit $\alpha \rightarrow \infty$ and $s \rightarrow 0$ is relevant to the magnetism of a material as predicted by meta-GGAs. It is also interesting to note that the same limit is also important for a semilocal functional to capture a portion of intermediate-range van der Waals interaction between weakly-overlapped densities [39].

In Fig. 10, we plot α as a function of distance from the V nucleus in R-VO₂. The radial factors of all-electron 3p and 3d orbitals for a free V⁺⁴ ion are also shown in the same figure. In the region $d < 0.2 \text{ \AA}$, α is very large, due to the pseudopotential approximation used in VASP calculations. In the range from 0.2 \AA to 0.5 \AA , we can see the overlap of 3p and 3d orbitals. In this region, α is also $\gg 1$. Moving outside further ($d > 0.7 \text{ \AA}$), we have $\alpha \approx 1$, and the density is more dominated by the 3d orbital. Fig. 10 suggests the relevance of $\alpha \gg 1$ to magnetism.

In order to further verify the correlation between magnetism and exchange enhancement factor of a meta-GGA functional, we have calculated the magnetic moment of Fe in the body-centered cubic (BCC) structure [63]. It is known that BCC Fe is a ferromagnetic metal below its Curie point (1043 K) with a large local moment as $2.22 \mu_B$ per atom [58]. In this case, the local moment is underestimated by LSDA ($1.94 \mu_B$), PBE ($2.17 \mu_B$), TPSS ($2.20 \mu_B$) and revTPSS ($2.19 \mu_B$) give results in good agreement with experiment. On the other hand, regTPSS ($2.46 \mu_B$), MGGA_MS0 ($2.63 \mu_B$), MGGA_MS2 ($2.62 \mu_B$), LSDA+U ($2.60 \mu_B$) and HSE06 ($2.82 \mu_B$) overestimate the value. We suggest that the over-prediction of the local magnetic moment in BCC Fe by regTPSS and two MGGA_MS variants is related to their exchange enhancement factors at large α and small s .

V. CONCLUSIONS

We have assessed the performances of several semilocal (LSDA, GGA and meta-GGAs), LSDA+U, and nonlocal (HSE06 and RPA) density functionals for the ground-state energy, electronic structure and magnetism of strongly-correlated R-VO₂. Our calculations indicate that all these functionals can predict the FM ground state for this metal oxide at low temperature, in agreement with a recent FN-DMC calculation. All semilocal functionals predict R-VO₂ to be a metallic ferromagnetic phase. However, LSDA+U and HSE06 incorrectly give a Mott-Hubbard insulating phase for R-VO₂ with large local magnetic moments. In addition, the TPSS and revTPSS meta-GGAs give qualitatively different (much more hybridized) electronic structures for R-VO₂ from those of either the widely-used LSDA and PBE functionals or the recently developed meta-GGA functionals (regTPSS and MGGA_MS family of density functionals),

possibly due to the order-of-limits error in TPSS and revTPSS. Using PBE inputs, the ground state of R-VO₂ is found to be a ferromagnetic metal by RPA. Full RPA selfconsistency might be required in some systems, especially strong-correlated ones.

For most semilocal functionals, the development of magnetic states (FM or AFM) gives more realistic equilibrium cell volumes than those of the spin-unpolarized state. This result suggests either that there really are temperature-disordered local spin moments in R-VO₂, or that spin-polarization is mimicking strong correlation (as it does in DFT calculations for equilibrium Cr₂ or stretched H₂ [36]). LSDA and RPA (with PBE inputs) behave differently, where for the former all three computed magnetic states (FM, AFM and spin compensated PM) underestimate the equilibrium cell volume with similar percent errors; while for the latter the optimized cell volume for a magnetic state is significantly overestimated.

In meta-GGAs, there is a correlation between the predicted magnetic moment and the behavior of the exchange enhancement factor. Our calculations for either R-VO₂ or BCC Fe tell the same story: The monotonic decrease of $F_x(s, \alpha)$ with α for small s results in a large local magnetic moment for the magnetic phase. Although the meta-GGAs exhibiting an exchange enhancement factor similar to MGGA_MS variants seem to be less accurate than other tested semilocal functionals for the local magnetic spin moments of R-VO₂, they are able to capture a portion of intermediate-range van der Waals interaction for the same reason that they predict too-large local magnetic moments.

From our work and the FN-DMC work of Ref. 14, it appears likely that the ground state of R-VO₂ would be magnetic, and that the observed paramagnetic state above the transition temperature (340 K) is one of temperature-disordered local spin moments. Some of the FN-DMC results find a very small energy difference between FM and AFM phases, suggesting that temperature could easily disorder the spins. It is a puzzle that the observed magnetic susceptibility of R-VO₂ [1, 15] does not seem to display the expected Curie-Weiss law. Perhaps in R-VO₂ below 340 K there is a thermal transition to the spin-compensated paramagnetic state.

After our manuscript was completed, we discovered Ref. 64, which shows that the range-separated hybrid HSE06 works better for VO₂ with 10% of exact exchange than with the standard 25%. With 10% of exact exchange, M-VO₂ properly remains an insulator while R-VO₂ is properly a ferromagnetic metal. We note that 25% of exact exchange (with 75% of PBE GGA exchange) is only a good average for molecules and semiconducting solids. Less or no exact exchange is needed in metals, and more than 25% is needed in large-gap insulators. The fraction of exact exchange should vary locally throughout any system, as it does in a local hybrid functional [65].

ACKNOWLEDGEMENTS

B. Xiao would like to acknowledge computational support from the Center for Computational Sciences (CCS) at Tulane University, where most of the DFT calculations have been performed. Some of the calculations were also conducted on the NERSC computational facilities and the High Performance Computing (HPC) cluster at Temple University. The authors also thank Prof. Jianmin Tao (University of Pennsylvania) and Prof. Lucas K. Wagner (University of Illinois at Urbana-Champaign) for fruitful discussions, as well as Abhirup Patra for Fig. 10. This work was supported by the National Science Foundation under Grant No. DMR-1305135, and also by the Department of Energy under Grant No. DE-SC0010499. This research used resources of the National Energy Research Scientific Computing Center, which is supported by the Office of Science of the U.S. Department of Energy under Contract No. DE-AC02-05CH11231.

REFERENCES

- [1] C.N. Berglund and H.J. Guggenheim, *Phys. Rev.* **185**, 1022 (1969).
- [2] V. Eyert, *Ann. Phys. (Leipzig)* **11**, 1 (2002).
- [3] M.A. Korotin, N.A. Skorikov and V.I. Anisimov, *Phys. of Metals and Metallography (USSR)* **94**, 17 (2002).
- [4] V. Eyert, *Phys. Rev. Lett.* **107**, 016401 (2011).
- [5] F. Gervais and W. Kress, *Phys. Rev. B* **31**, 4809 (1995).
- [6] J.B. Goodenough, *J. Solid. State. Chem.* **3**, 490 (1971).
- [7] K. Okazaki, A. Fujimori and M. Onoda, *J. Phys. Soc. Jpn.* **71**, 822 (2002).
- [8] A. Cavalleri, Th. Dekorsy, H.H.W. Chong, J.C. Kieffer and R.W. Schoenlein, *Phys. Rev. B* **70**, 161102 (2004).
- [9] Y. Muraoka, Y. Ueda and Z. Hiroi, *J. Phys. Chem. Solids.* **63**, 965 (2002).
- [10] M.W. Haverkort, Z. Hu, L.H. Tjeng, A. Tanaka, H.H. Hsieh, H.J. Lin and C.T. Chen, *Phys. Rev. Lett.* **95**, 196404 (2005).
- [11] A. Liebsch, H. Ishida and G. Bihlmayer, *Phys. Rev. B* **71**, 085109 (2005).
- [12] R. Grau-Crespo, H. Wang and U. Schwingenschlöggl, *Phys. Rev. B* **86**, 081101 (2012).
- [13] M. Gatti, F. Bruneval, V. Olevano and L. Reining, *Phys. Rev. Lett.* **99**, 266402 (2007).
- [14] H. Zheng and L.K. Wagner, arXiv:1310.1066 (2014) and private communication.

- [15] J.P. Pouget, P. Lederer and D.S. Schreiber, *J. Phys. Chem. Solids*. **33**, 1961 (1972).
- [16] J.P. Perdew, S. Kurth, A. Zupan and P. Blaha, *Phys. Rev. Lett.* **82**, 2544 (1999).
- [17] V.N. Staroverov, G.E. Scuseria, J. Tao and J.P. Perdew, *Phys. Rev. B* **69**, 075102 (2004).
- [18] D.C. Langreth and J.P. Perdew, *Phys. Rev. B* **21**, 569 (1980).
- [19] Y. Zhao and D.G. Truhlar, *J. Chem. Phys.* **125**, 194101 (2006).
- [20] J. Tao, J.P. Perdew, V.N. Staroverov and G. E. Scuseria, *Phys. Rev. Lett.* **91**, 146401 (2003).
- [21] V.N. Staroverov, G. E. Scuseria, J. Tao and J.P. Perdew, *J. Chem. Phys.* **119**, 12129 (2003).
- [22] J.P. Perdew, A. Ruzsinszky, G.I. Csonka, L.A. Constantin and J. Sun, *Phys. Rev. Lett.* **103**, 026403 (2009).
- [23] P. Haas, F. Tran and P. Blaha, *Phys. Rev. B* **79**, 085104 (2009).
- [24] P. Hao, Y. Fang, J. Sun, G.I. Csonka, P.H.T. Philipsen and J.P. Perdew, *Phys. Rev. B* **85**, 014111 (2012).
- [25] C. Rödl, F. Fuchs, J. Furthmüller and F. Bechstedt, *Phys. Rev. B* **79**, 235114 (2009).
- [26] F. Tran, P. Blaha, K. Schwarz and P. Novák, *Phys. Rev. B* **74**, 155108 (2006).
- [27] B. Xiao, J. Sun, A. Ruzsinszky, J. Feng and J.P. Perdew, *Phys. Rev. B* **86**, 094109 (2012).
- [28] L. Schimka, J. Harl, A. Stroppa, A. Grüneis, M. Marsman, F. Mittendorfer and G. Kresse, *Nature Materials*, **9**, 741 (2010).
- [29] T. Olsen, J. Yan, J.J. Mortensen and K.S. Thygesen, *Phys. Rev. Lett.* **107**, 156401 (2011).
- [30] F. Mittendorfer, A. Garhofer, J. Redinger, J. Klimeš, J. Harl and G. Kresse, *Phys. Rev. B* **84**, 201401 (R) (2011).
- [31] H. Peng and S. Lany, *Phys. Rev. B* **87**, 174113 (2013).
- [32] L. Schimka, R. Gaudoin, J. Klimeš, M. Marsman and G. Kresse, *Phys. Rev. B* **87**, 214102 (2013).
- [33] A. Heßelmann and A. Görling, *Mol. Phys.* **109**, 2473 (2011).
- [34] H. Eshuis, J.E. Bates and F. Furche, *Theor. Chem. Acc.* **131**, 1084 (2012).
- [35] X. Ren, P. Rinke, C. Joas and M. Scheffler, *J. Mater. Sci.* **47**, 7447 (2012).
- [36] J.P. Perdew, A. Savin, and K. Burke, *Phys. Rev. A* **51**, 4531 (1995).

- [37] J. Sun, B. Xiao and A. Ruzsinszky, J. Chem. Phys. **137**, 051101 (2012).
- [38] J. Sun, R. Haunschild, B. Xiao, I.W. Bulik, G.E. Scuseria and J.P. Perdew, J. Chem. Phys. **138**, 044113 (2013).
- [39] J. Sun, B. Xiao, Y. Fang, R. Haunschild, P. Hao, A. Ruzsinszky, G.I. Csonka, G.E. Scuseria and J.P. Perdew, Phys. Rev. Lett. **111**, 106401 (2013).
- [40] Y. Fang, B. Xiao, J. Tao, J. Sun and J.P. Perdew, Phys. Rev. B **87**, 214101 (2013).
- [41] The total energies of M-VO₂ were also calculated in FM, AFM and PM states using the *vasp* program by LSDA, PBE, and meta-GGAs (TPSS, revTPSS, regTPSS and MGGA_MS2) with the experimental lattice constants. Experimentally, M-VO₂ is the ground phase of VO₂ at low temperature. Other than MGGA_MS2, the tested exchange-correlation functionals always predict that the total energies of R-VO₂ are lower than those of M-VO₂. Only in FM and AFM states does MGGA_MS2 find that M-VO₂ has lower total energies than R-VO₂. MGGA_MS2 still gives the wrong phase stability order of R- and M-VO₂ in the PM state.
- [42] G. Kresse and J. Furthmüller, Phys. Rev. B **54**, 11169 (1996).
- [43] H.J. Monkhorst and J.D. Pack, Phys. Rev. B **13**, 5188 (1976).
- [44] A. Ruzsinszky, J. Sun, B. Xiao and G.I. Csonka, J. Chem. Theory Comput. **8**, 2078 (2012).
- [45] J.P. Perdew and A. Zunger, Phys. Rev. B **23**, 5048 (1981).
- [46] J.P. Perdew, K. Burke and M. Ernzerhof, Phys. Rev. Lett. **77**, 3865 (1996).
- [47] V.I. Anisimov, J. Zaanen and O.K. Andersen, Phys. Rev. B **44**, 943 (1991).
- [48] S.L. Dudarev, G.A. Botton, S.Y. Savrasov, C.J. Humphreys and A.P. Sutton, Phys. Rev. B **57**, 1505 (1998).
- [49] S. Biermann, A. Poteryaev, A.I. Lichtenstein and A. Georges, Phys. Rev. Lett. **94**, 026404 (2005).
- [50] J. Heyd, G.E. Scuseria and M. Ernzerhof, J. Chem. Phys. **118**, 8207 (2003). J. Heyd, G.E. Scuseria, and M. Ernzerhof, J. Chem. Phys. **124**, 219906 (2006).
- [51] A.V. Krukau, O.A. Vydrov, A.F. Izmaylov and G.E. Scuseria, J. Chem. Phys. **125**, 224106 (2006).
- [52] K. Hummer, J. Harl and G. Kresse, Phys. Rev. B **80**, 115205 (2009).
- [53] J. Wróbel, K.J. Kurzydłowski, K. Hummer, G. Kresse and J. Piechota, Phys. Rev. B **80**, 155124 (2009).

- [54] J. Harl, L. Schimka and G. Kresse, Phys. Rev. B **81**, 115216 (2010).
- [55] J. Harl and G. Kresse, Phys. Rev. B **77**, 045136 (2008).
- [56] Supplementary Materials: The convergence tests for the RPA calculations are explained for the computed energy differences between the magnetic phases (FM and AFM) and the spin compensated non-magnetic phase. The computed energy versus volume curves using RPA based on PBE geometry are given for FM, AFM and non-magnetic R-VO₂ phases. The energy differences are recalculated using the fully relaxed R-VO₂ structures by semilocal and nonlocal functionals. The band energies and widths are given for 2s, 2p and 3d states in FM, AFM and spin compensated PM states. The band structures and electronic densities of states of AFM, FM and PM states are shown for other DFT methods. The atomic and orbital occupations are also presented for the tested DFT methods.
- [57] M.E. Williams, W.H. Butler, C.K. Mewes, H. Sims, M. Chshiev, S.K. Sarker, J. Appl. Phys. **105**, 07E510 (2009).
- [58] J. Sun, M. Marsman, G. Csonka, A. Ruzsinszky, P. Hao, Y.S. Kim, G. Kresse and J.P. Perdew, Phys. Rev. B **84**, 035117 (2011)
- [59] P.I. Sorantin and K. Schwarz, Inorg. Chem. **31**, 567 (1991).
- [60] T. Kotani and H. Akai, J. Magn. Magn. Mater. **177-181**, 569 (1998).
- [61] T. Kotani, J.Phys.: Condens. Matter. **10**, 9241 (1998).
- [62] A.M. Rappe, K.M. Rabe, E. Kaxiras and J.D. Joannopoulos, Phys. Rev. B **41**, 1227 (1990).
- [63] The calculations for BCC Fe were performed in the VASP code. We employed 500 eV for the kinetic energy cutoff and a 16×16×16 k-mesh generated automatically by the Monkhorst-Pack method. The BCC Fe geometry was fully relaxed by each DFT method self-consistently. Then, the local moment was computed using the optimized structure.
- [64] H. Wang, T.A. Mellan, R. Grau-Crespo, and U. Schwingenschlögl, Chem. Phys. Lett. **608**, 126 (2014).
- [65] J.P. Perdew, V.N. Staroverov, J. Tao, and G.E. Scuseria, Phys. Rev. A **78**, 052513 (2008).

Figure Captions

FIG. 1. (Color online) The two magnetic states of rutile-type VO_2 . (a): Ferromagnetic state (FM); (b): Antiferromagnetic state (AFM). Note that the big blue balls are V atoms and the small red ones are O atoms, respectively. The **green solid arrows** represent the directions of local magnetic moments of V atoms. The octahedra represent VO_6 structural units.

FIG. 2. (Color online) (a): The relationship between global crystallographic coordinates (X-Y-Z) and local coordinates (x-y-z) of V atoms; (b): The irreducible representations of 3d orbitals in O_h and D_{4h} point groups under the local coordinate system (x-y-z).

FIG. 3. (Color online) The energy differences between two magnetic states (FM and AFM) and the spin-compensated non-magnetic state are calculated using the experimental lattice constants (Expt, **see also Table I for the precise values**) and fully relaxed geometry (Opt) **in frames (a) and (b), respectively. The energy difference between FM and AFM states is given in frame (c).** Note that for RPA the values marked as “Opt” are obtained by minimizing the total energy with respect to the PBE cell volume. The FN-DMC calculation of Ref. [14] predicts -300 meV/ VO_2 for FM-PM and **AFM-PM.**

FIG. 4. (Color online) The computed local magnetic moments of V atoms by different exchange-correlation functionals. The horizontal line represents the exact value of the local magnetic moment carried by a free V^{4+} cation. (a): FM; (b): AFM. The fractional coordinates for V_I and V_{II} are (0, 0, 0) and (0.5, 0.5, 0.5), respectively.

FIG. 5. (Color online) The weighted up-spin band dispersions of FM rutile-type VO_2 calculated by semilocal functionals and also HSE06. The size of the black dots represents the weights of 3d orbitals of V atoms. The solid blue lines are the energy bands of bulk R- VO_2 . The fractional coordinates for these special high-symmetry k points are Z (0, 0, 1/2), A (1/2, 1/2, 1/2), M (1/2, 1/2, 0), Γ (0, 0, 0), R (0, 1/2, 1/2) and X (0, 1/2, 0). (a): PBE; (b): TPSS; (c): MGGA_MS2; (d): HSE06. The Fermi level is set to zero at the top of the valence band.

FIG. 6. (Color online) The relative positions of O 2s bands computed by semilocal functionals in FM and AFM states. The 2s band positions obtained from LSDA are set to zero. The value of $F_x(s, \alpha)$ is evaluated with the assumption that $s \rightarrow 0$ and $\alpha = 0$ for the spherical-like single orbital region.

FIG. 7. (Color online) The calculated spin-polarized density of states of FM rutile-type VO_2 from different exchange-correlation functionals. The angular-momentum-projected densities of states on to 3d orbitals are also shown for the up-spin direction. The vertical line refers to the Fermi level. (a): PBE; (b): TPSS; (c): MGGA_MS2; (d): HSE06. The notations for five 3d states of the V atom are defined in crystallographic Cartesian coordinates (X-Y-Z).

FIG. 8. (Color online) The computed percent errors of equilibrium cell volume in three different magnetic states by semilocal and nonlocal functionals. For RPA, the equilibrium cell volume is obtained by fitting the total energy versus volume curve to the equation of state.

FIG. 9. (Color online) The α dependence of meta-GGA exchange enhancement factors for different s values. LDA and PBE are represented by horizontal lines, because both exchange functionals show no dependence on α .

FIG. 10. (Color online) Position dependence of α near a V nucleus in R-VO₂. The all-electron 3p and 3d orbitals for a free V⁺⁴ ion, in arbitrary units, are also shown. These orbitals are obtained by solving the non-relativistic Schrödinger equations using PBE for the exchange-correlation energy in the OPIUM code [62].

Tables

Table I The relative stabilities of ferromagnetic (FM) and anti-ferromagnetic (AFM) states with respect to the spin-compensated paramagnetic (PM) state of the R-VO₂ structure. The energy difference between FM and AFM states is indicated by FM-AFM. The energy differences are computed using the experimental lattice constants with the optimized atomic positions. For RPA, the PBE inputs are used in the calculations. The unit for the calculated energies is meV/VO₂. The FN-DMC calculation of Ref. [14] predicts -300 for FM-PM and AFM-PM.

Magnetism	LSDA	LSDA+U	PBE	TPSS	revTPSS	regTPSS	MGGA_MS0	MGGA_MS2	HSE06	RPA
FM	-33.5	-827.4	-100.7	-95.2	-103.7	-115.6	-275.1	-196.9	-826.1	-85.9
									-739.0 ^a	
AFM	-0.4	-834.8	-8.1	-5.0	-5.8	-7.8	-104.4	-49.7	-568.0	-43.2
									-700.0 ^a	
FM-AFM	-33.1	7.4	-92.6	-90.3	-97.9	-107.8	-170.7	-147.3	-258.1	-42.6
									-39.0 ^a	

^aReference [12].

Figures

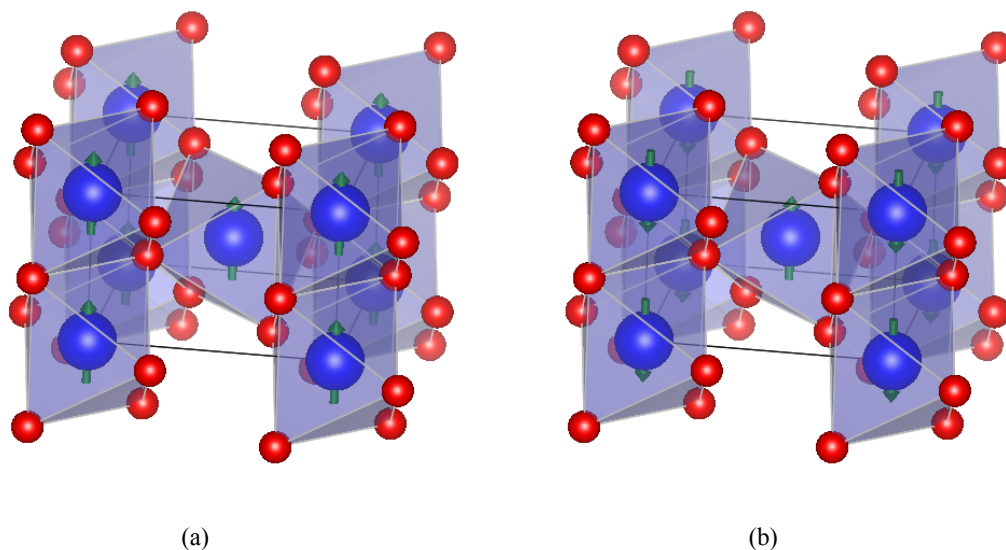


FIG. 1. (Color online) The two magnetic states of rutile-type VO_2 . (a): Ferromagnetic state (FM); (b): Antiferromagnetic state (AFM). Note that the big blue balls are V atoms and the small red ones are O atoms, respectively. The green solid arrows represent the directions of local magnetic moments of V atoms. The octahedra represent VO_6 structural units.

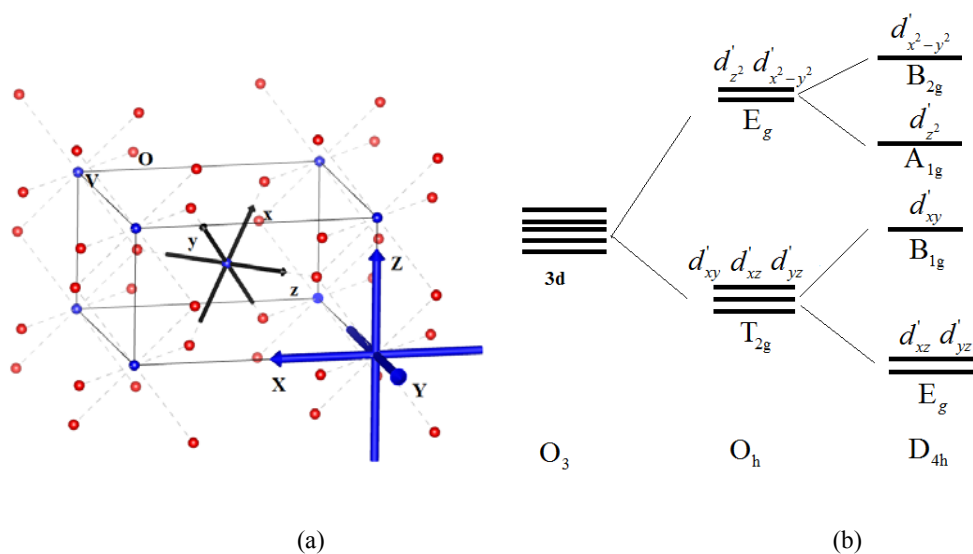


FIG. 2. (Color online) (a): The relationship between global crystallographic coordinates (X-Y-Z) and local coordinates (x-y-z) of V atoms; (b): The irreducible representations of 3d orbitals in O_h and D_{4h} point groups under the local coordinate system (x-y-z).

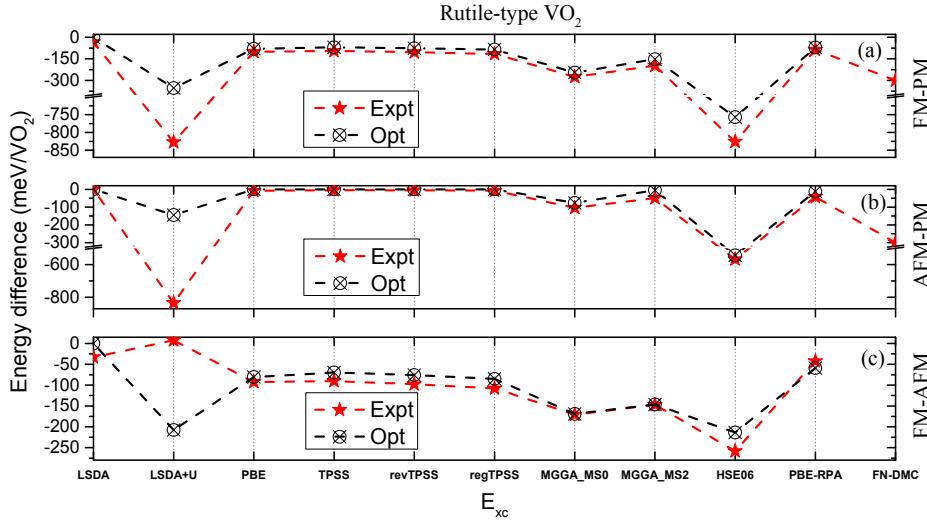


FIG. 3. (Color online) The energy differences between two magnetic states (FM and AFM) and the spin-compensated non-magnetic state are calculated using the experimental lattice constants (Expt, see also Table I for the precise values) and fully relaxed (Opt) geometry in frames (a) and (b), respectively. The energy difference between FM and AFM states is given in frame (c). Note that for RPA the values marked as “Opt” are obtained by minimizing the total energy with respect to the PBE cell volume. The FN-DMC calculation of Ref. 14 predicts -300 meV/VO₂ for FM-PM and AFM-PM.

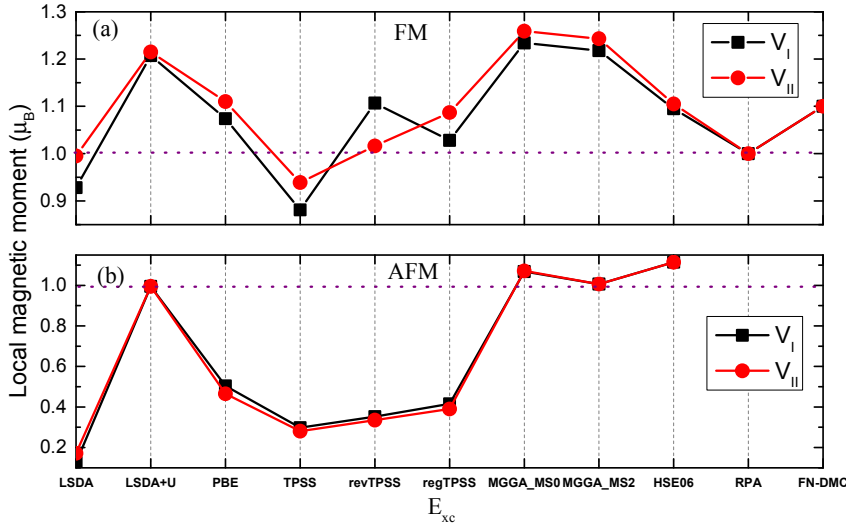


FIG. 4. (Color online) The computed local magnetic moments of V atoms by different exchange-correlation functionals. The horizontal line represents the exact value of the local magnetic moment carried by a free V⁴⁺ cation. (a): FM; (b): AFM. The fractional coordinates for V_I and V_{II} are (0, 0, 0) and (0.5, 0.5, 0.5), respectively.

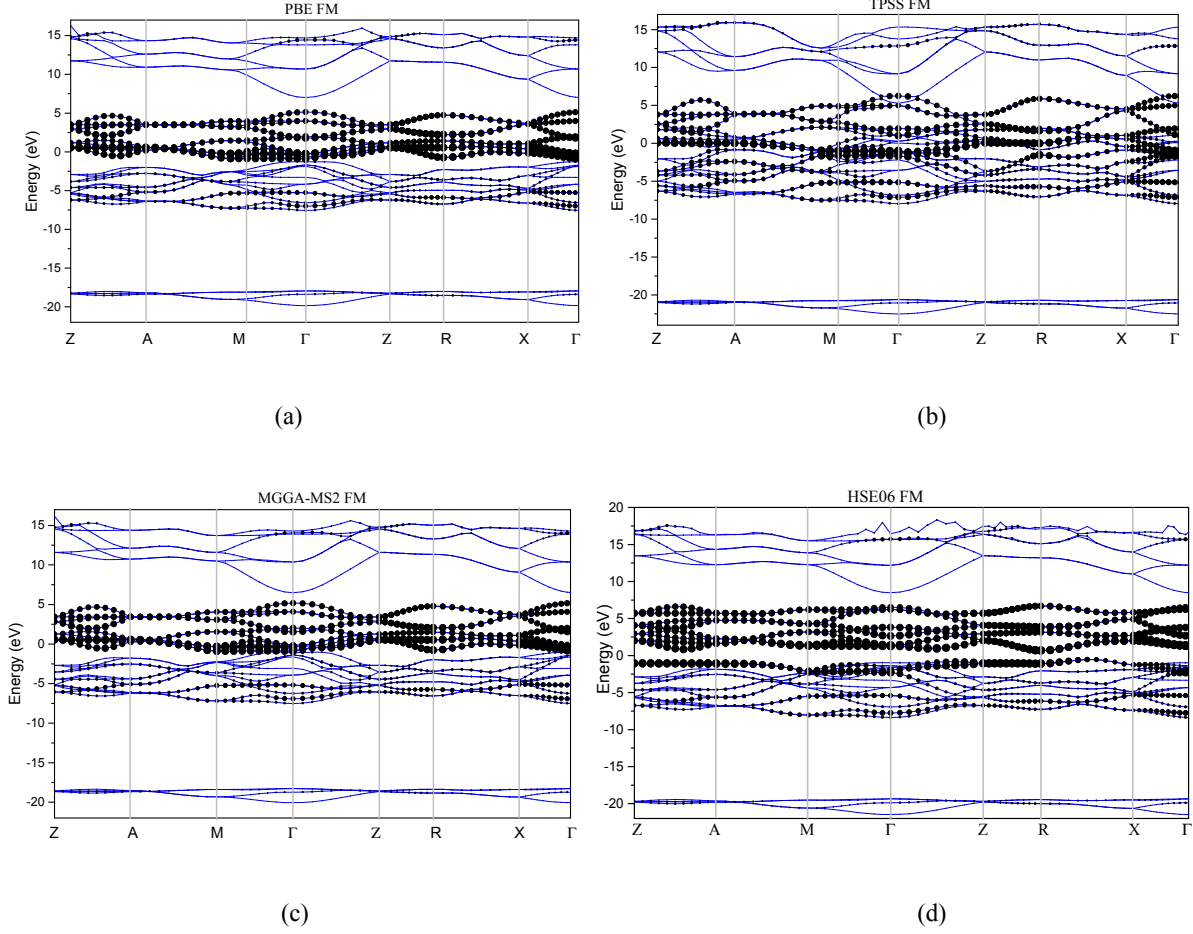


FIG. 5. (Color online) The weighted up-spin band dispersions of FM rutile-type VO_2 calculated by semilocal functionals and also HSE06. The size of the black dots represents the weights of 3d orbitals of V atoms. The solid blue lines are the energy bands of bulk R- VO_2 . The fractional coordinates for these special high-symmetry k points are Z (0, 0, 1/2), A (1/2, 1/2, 1/2), M (1/2, 1/2, 0), Γ (0, 0, 0), R (0, 1/2, 1/2) and X (0, 1/2, 0). (a): PBE; (b): TPSS; (c): MGGA_MS2; (d): HSE06. The Fermi level is set to zero at the top of the valence band.

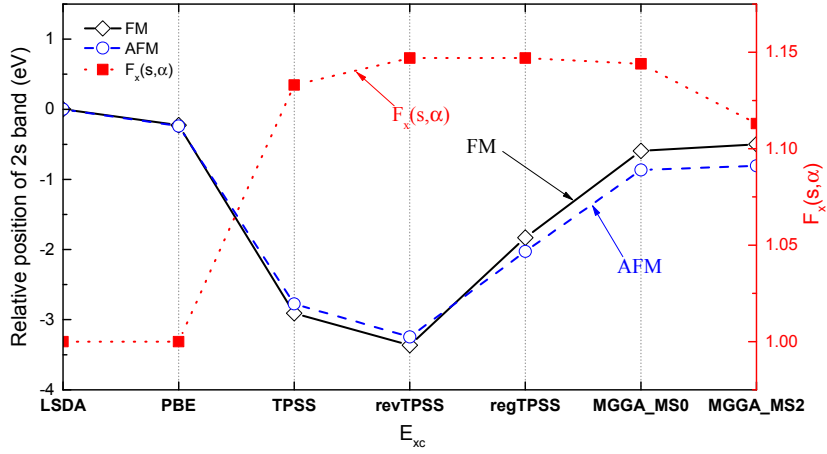
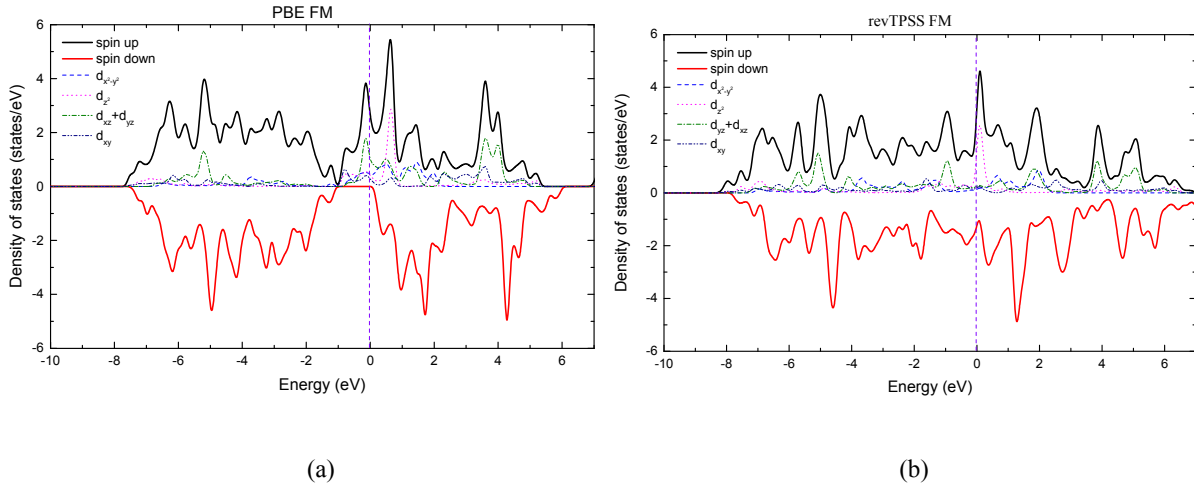


FIG. 6. (Color online) The relative positions of O 2s bands computed by semilocal functionals in FM and AFM states. The 2s band positions obtained from LSDA are set to zero. The value of $F_x(s, \alpha)$ is evaluated with the assumptions that $s \rightarrow 0$ and $\alpha = 0$ for the spherical-like single orbital region.



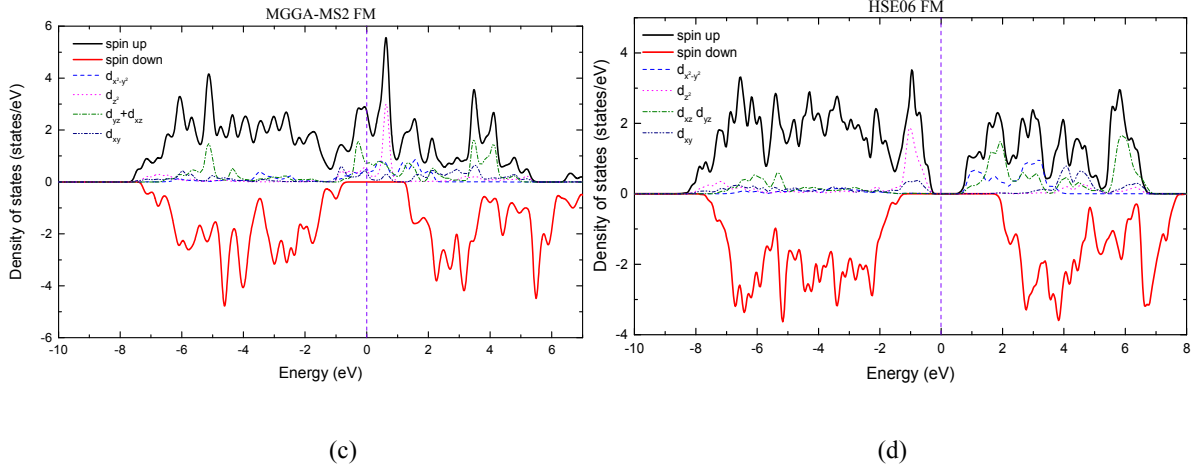


FIG. 7. (Color online) The calculated spin-polarized density of states of FM rutile-type VO_2 from different exchange-correlation functionals. The angular-momentum-projected densities of states on to 3d orbitals are also shown for the up-spin direction. The vertical line refers to the Fermi level. (a): PBE; (b): TPSS; (c): MGGA_MS2; (d): HSE06. The notations for five 3d states of the V atom are defined in crystallographic Cartesian coordinates (X-Y-Z).

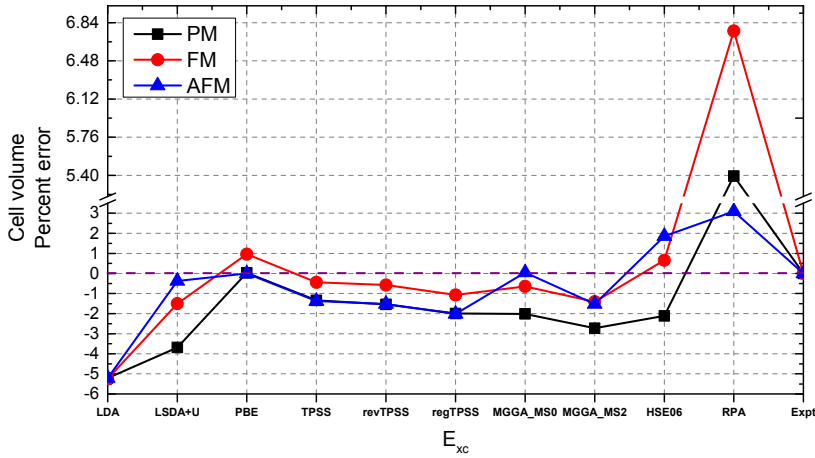
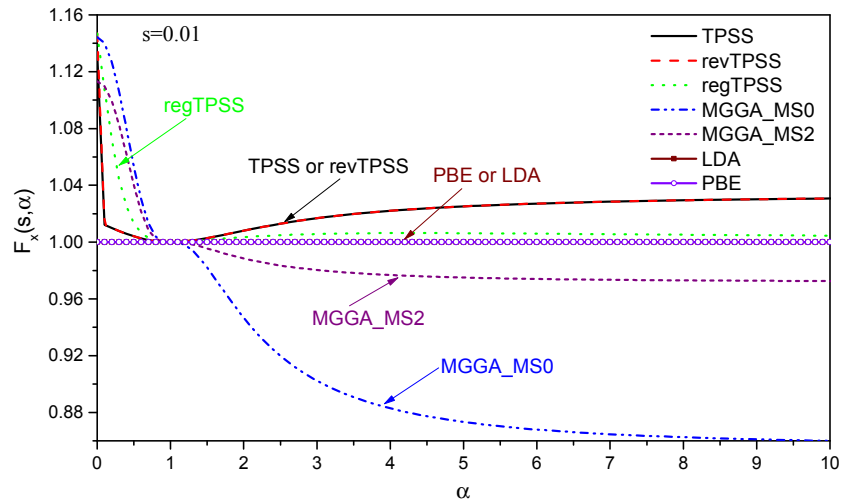
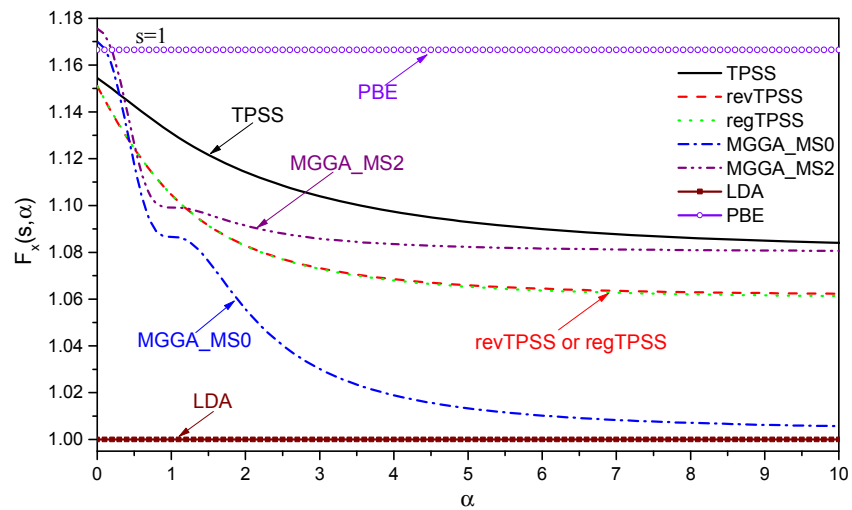


FIG. 8. (Color online) The computed percent errors of equilibrium cell volume in three different magnetic states by semilocal and nonlocal functionals. For RPA, the equilibrium cell volume is obtained by fitting the total energy versus volume curve to the equation of state.



(a)



(b)

FIG. 9. (Color online) The α dependence of meta-GGA exchange enhancement factors for different s values. LDA and PBE are represented by horizontal lines, because both exchange functionals show no dependence on α .

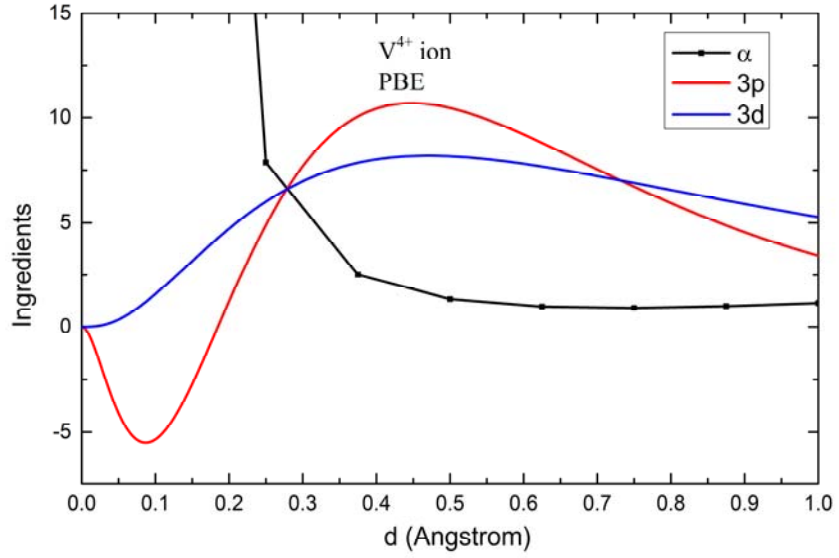


FIG. 10. (Color online) Position dependence of α near a V nucleus in R-VO₂. The all-electron 3p and 3d orbitals for a free V⁴⁺ ion, in arbitrary units, are also shown. The orbitals are obtained by solving the non-relativistic Schrödinger equations using PBE for the exchange-correlation energy in the OPIUM code [62].